the surface of an object but does not measure the absolute temperature.

To enhance our observational capability during the eruption of Mount St. Helens, we also used a precision infrared radiation thermometer (*1*) to measure the apparent temperature and calculate (*6*) the actual temperature of the plumes associated with the eruptions. This machine was used by Birnie (*6*) in his study of Guatemalan volcanoes and by Lange and Avent (*7*) in examining the thermal properties of Mount Lassen. We also had a seismograph (Sprengnether MEQ) with a 1-Hz seismometer in operation to correlate seismic and thermal activity.

During our survey of Mount St. Helens in August 1979 we used the thermal infrared scanner to survey the northern half of the mountain. At that time, we found no indication of thermal anomalies. However, an airborne infrared survey of the mountain in 1966 (*4*) delineated a warm area on the northwestern side of the mountain 1/2 km from the summit in a zone designated as "the Boot" on the U.S. Geological Survey Mount St. Helens quadrangle. In 1941, mountaineers described several small fumaroles and a large area of warm rock on the Boot (*4*). Our visual observations during the 1980 eruptive period showed that the Boot was covered with snow, suggesting that the heat flow from this area is small. The snow cover coupled with our low angle of view of the mountain may account for our failure to detect a thermal anomaly on the Boot during our 1979 survey. Alternatively, it is possible that the Boot has cooled since the 1966 aerial survey. From our observation post 9 km from the mountain, our minimum area of resolution was approximately 100 m^2. Hence, a small thermal area might not be detected. Another area of interest to us during our 1979 survey was the "Goat Rock" dome, a side vent that formed during the last century on the northwestern side of the mountain 2 km from the summit. As with our observation of the Boot, we found no indication of a thermal anomaly at this site (*8*).

On 2 April 1980, we made an overflight of the mountain to examine the crater region with the infrared scanner. At that time, we also observed the volcano's south side, which we could not see from our ground-based observation post. Measurements from our overflight of the mountain substantiated our ground-based observations. Although we examined the crater region during the day, which is not optimal for infrared scanning because of the solar radiation effects, we found no evidence of large temperature differences in the crater (*9*).

The eruptions of Mount St. Helens during the period from 30 March to 4 April varied from small puffs of steam lasting a few seconds to large plumes of ash and steam lasting up to 35 minutes. Most eruptions ended abruptly. The time between successive eruptions varied from 30 minutes to 4 hours, the quiescent time increasing through the week along with the average length of the eruptions. The longer eruptions often showed distinct phases. During the first phase only steam was vented; after several minutes dark bursts of ash and steam would appear and continue until the end of the eruption.

In examining the eruptive plumes, we found no evidence of significant temperature differences within the ejecta as it left the crater. Using the infrared thermometer, we calculated plume temperatures 100 m above the crater to be only slightly higher than the ambient temperature. Generally the apparent plume temperatures ranged from 5° to 15°C. The mean temperature of the plumes rose 10°C over the period of our observation. Using the infrared scanner, we found that after the eruption the plume cooled to ambient-air temperature within a few minutes.

A comparison of our infrared data from the summer of 1979 with that from the 1980 eruption sequence indicates that there was no significant change in surface temperatures. In neither survey did we find any major rise in temperature (on the order of 1°C) over any part of the mountain. This result suggests that there was no noticeable increase in heat flow at the surface of Mount St. Helens prior to the initial phreatic eruptions. Moreover, there was no visible evidence of rapid melting of the seasonal snow on any part of the mountain, at least up until 4 April 1980. This evidence of little or no preheating is perplexing in view of observations of increased heat flow on Mount Baker (*5*) and Mount Wrangell (*10*), both of which have warmed significantly but have not erupted.

WILLIAM ST. LAWRENCE
U.S. Army Cold Regions Research
and Engineering Laboratory,
Hanover, New Hampshire 03755

ANTHONY QAMAR
JOHNNIE MOORE
GEORGE KENDRICK
Department of Geology,
University of Montana, Missoula 59812

References and Notes

1. The thermal scanner (AGA Corporation, Thermovision 750) has a spectral range of 2.0 to 5.6 μm. The angle of view is 20° with the regular lens and 7° with the telephoto lens. Each picture element making up the image in the cathode-ray tube subtends 0.06° (telephoto lens). The sensitivity is 0.2°C. The infrared thermometer (Barnes Engineering Company, PRT-5) has a spectral range of 9.5 to 11.5 μm and an angle of view of 0.4°. The sensitivity is about 0.1°C.
2. D. R. Crandell *et al.*, *Science* **187**, 438 (1975).
3. D. R. Crandell and D. R. Mullineaux, *U.S. Geol. Surv. Bull. 1383-C* (1978).
4. R. M. Moxham, *Bull. Volcanol.* **34**, 77 (1970).
5. D. Frank, M. F. Meier, D. A. Swanson, *U.S. Geol. Surv. Prof. Pap. 1022-A* (1977).
6. R. W. Birnie, *Bull. Volcanol.* **37**, 1 (1972).
7. I. M. Lange and J. C. Avent, *Science* **182**, 279 (1973).
8. We were able to establish confidence in our infrared method when we successfully located hot areas near the summit of Mount Shasta and on the lower, north flank of Mount Lassen.
9. In our aerial survey the instrument was set to detect temperature differences of 100°C to overcome any daytime solar-heating effects.
10. C. S. Benson and R. J. Motyka, "Annual Report" (Geophysical Institute, University of Alaska, Fairbanks, 1977–78).
11. We thank the National Broadcasting Corporation and I. Lange for arranging a helicopter flight over Mount St. Helens. We also thank the U.S. Geological Survey and the U.S. Forest Service for allowing us to establish our observation post.

23 May 1980; revised 11 July 1980

Oxygen Consumption in Pelagic Marine Sediments

Abstract. *Measurements in the interstitial waters of pelagic red clay and carbonate ooze sediments in the central equatorial Pacific show that the dissolved oxygen content decreases with depth and levels off at nonzero values. The supply of reactive organic carbon introduced by bioturbation limits oxygen consumption at depth in the sediment. These gradients should produce diffusive fluxes across the sediment-water interface that average about* 8.8×10^{-14} *mole per square centimeter per second or 0.08 milliliter per square meter per hour.*

Pelagic sediments, which cover most of the ocean basin floor, are assumed to be aerobic because of the low supply of organic matter to the sediments and their slow rate of sedimentation. The presence of dissolved oxygen (O_2) in the sediments has been inferred on the basis of the distribution of other chemical species such as NO_3^- (*1*). The O_2 content is the critical measurement because O_2 is the electron acceptor thermodynamically favored by heterotrophic bacteria (*2*). We have developed a method for collecting and analyzing interstitial water samples uncontaminated with atmospheric O_2. Our data confirm that O_2 is present throughout the top 50 cm of some equatorial red clay and carbonate ooze sediments. The profiles can be used to calculate the diffusive flux of O_2 through the

0036-8075/80/0926-1527$00.50/0

Table 1. Diffusive O_2 fluxes from bottom water into red clay (RC) and carbonate ooze (CO) sediments from different depths in the central equatorial Pacific. An average diffusion coefficient of 6.0×10^{-6} cm^{-2} sec^{-1} was used.

Station	Water depth (m)	Sediment type	B (cm^{-1})	ΔO_2 ($\times 10^{-8}$ mole cm^{-3})	Flux ($\times 10^{-14}$ mole cm^{-2} sec^{-1})	Flux (ml m^{-2} hour^{-1})
A	4239	CO	0.17	3.8	3.9	0.02
E	5269	RC	.31	8.2	1.5	.12
F	5867	RC	.089	5.6	3.0	.02
G	3572	CO	.058	7.9	2.8	.02
H	5352	RC	.17	8.9	8.4	.06
I	4765	CO	.19	12.5	14.4	.12
J	5361	RC	.20	12.8	15.6	.12
K	5469	RC	.32	13.1	25.1	.20
P	4822	CO	.10	8.2	4.4	.03
Average					8.8 ± 8.0	0.08 ± 0.06

sediment-water interface from the overlying water into the sediments.

We collected interstitial water samples, using a modified version of the in situ sampler designed by Sayles *et al.* (*3*). Calibrated sample loops (volume approximately 4 ml) of 0.32-cm nylon pressure tubing on six-port rotary valves were installed in line between the sampling port and the slave cylinders so that they were filled during collection of the interstitial water in situ. When the sampler was on deck, the valves were closed and the sample loops were removed and interfaced directly to a gas chromatograph (*4*). The accuracy and precision of our dissolved O_2 analyses were both about ± 2 percent (*5*). Samples were collected at nine stations in the equatorial Pacific during cruise 73 of the R.V. *Knorr* (Fig. 1).

The O_2 concentration of interstitial water decreases with increasing depth in the sediments at every station sampled (both red clay and carbonate ooze stations). This decrease indicates O_2 consumption in the sediments below the sediment-water interface. At some stations the decrease is relatively rapid, and most of the change in O_2 concentration is complete in the upper 5 to 10 cm (station J, Fig. 2). At other stations the decrease is much more gradual and occurs over the entire sampling interval (station G, Fig. 2). In some cases, the profiles in the sediments extrapolate up to bottom water concentrations within the limits of sample spacing and the precision of the analysis. In other cases, the data may exhibit an asymptotic approach to 40 to 60 percent of bottom water values.

Although there are differences in the shapes of the O_2 profiles, they have certain common features. The O_2 concentrations do not reach zero at any depth in the sampling interval at any of the stations. Instead, they level off or appear to be approaching some constant nonzero value. This value varies from station to station but is never less than 50 μmole kg^{-1}. The O_2 profiles from all stations show a more or less exponential decrease with depth.

For the purpose of comparing the shapes of the different O_2 profiles and for calculating diffusive fluxes of O_2 into the sediments, an exponential equation of the form

$$O_2(z) = O_2' + \Delta O_2 \exp(-Bz) \qquad (1)$$

was fitted to the data from each station. The term ΔO_2 is the total decrease in the O_2 concentration from the interface to the depth where it levels off at some constant value (O_2'); z is depth, and B is a constant but has physical significance as shown below.

If we consider a steady-state system with constant porosity and ignore burial

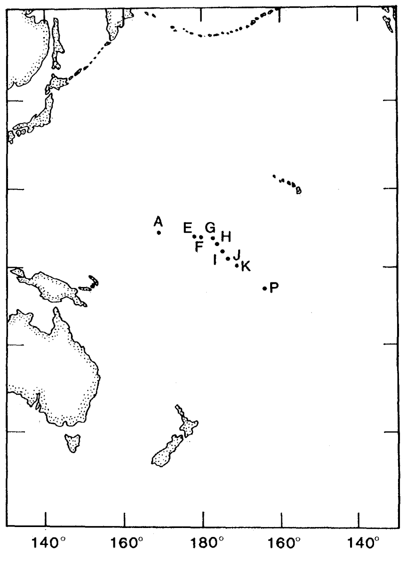

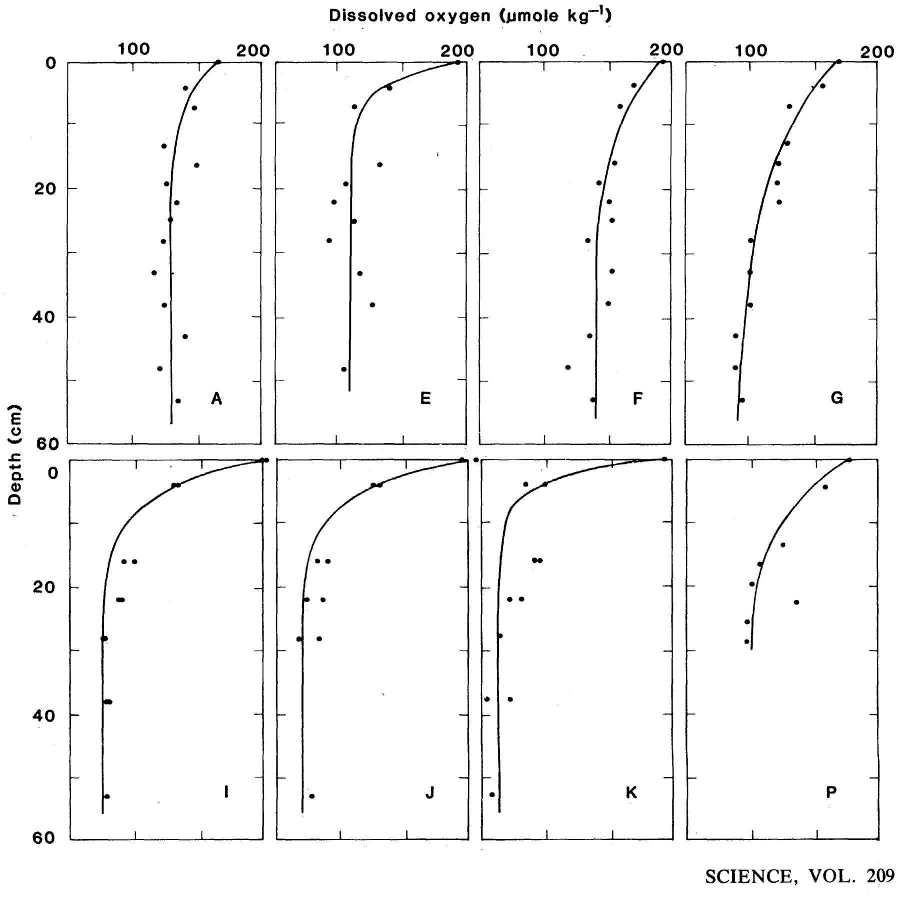

Fig. 1 (left). Station locations sampled during *Knorr* cruise 73 (July to August 1978). Fig. 2 (right). Vertical distribution of dissolved O_2 in the sediments at stations A, E, F, G, I, J, K, and P. The solid lines represent the fit of Eq. 1 to the actual data points by minimizing the variance of the actual data points from an exponential curve. An additional constraint is that the O_2 content equals that of bottom water at $z = 0$.

advection, the distribution of dissolved O_2 in the interstitial water of pelagic sediments will be controlled by a balance between the downward diffusive flux and consumption as a result of respiration:

$$D\frac{\partial^2 O_2}{\partial z^2} - \left(\frac{\partial O_2}{\partial t}\right)_{\text{resp}} = 0 \qquad (2)$$

The respiration term can be approximated by a first-order consumption proportional to the solid organic carbon (6),

$$\left(\frac{\partial O_2}{\partial t}\right)_{\text{resp}} = kC \qquad (3)$$

where C is the concentration of solid organic carbon at any depth, and k is a first-order rate constant.

The distribution of solid organic carbon with depth within the zone of bioturbation can be described by

$$K\frac{\partial^2 C}{\partial z^2} - w\frac{\partial C}{\partial z} - kC = 0 \qquad (4)$$

where K is the bioturbation mixing coefficient, and w is the sedimentation rate. Solution of Eq. 4 for the boundary conditions

$$z = 0,\ C = C_0$$
$$z \rightarrow \infty,\ C \rightarrow 0$$

leads to the expression [see (6)]

$$C = C_0 \exp\left\{\left[\frac{w - (w^2 + 4kK)^{1/2}}{2K}\right]z\right\} \qquad (5)$$

Thus B in Eq. 1 is given by

$$B = -\frac{w - (w^2 + 4kK)^{1/2}}{2K} \qquad (6)$$

For our observed values of B (Table 1) and representative values for the total sedimentation rate (0.1 to 2.0 cm per 1000 years) (7) and biological mixing coefficients (1 to 10^3 cm^2 per 1000 years) (8), it is clear that, near the sediment-water interface where the O_2 gradient is steepest, bioturbation will control the flux of organic carbon down into the sediments and thus the rate of O_2 consumption.

We fitted the O_2 data from each station to Eq. 1 by minimizing the variance of the actual data points from an exponential curve. The values of B and ΔO_2 for each of the stations are summarized in Table 1. Larger values of B mean a more rapid approach to O_2'. There are no gross differences in ΔO_2 or B between the carbonate ooze and red clay stations. The values of ΔO_2 do seem to show the same trend as the surface organic carbon values, which are largest in the equatorial region (9). If the steady-state diagenetic model holds, this implies that the value of B is approximately the same in red clay and carbonate ooze sediments despite the fact that carbonate ooze sediments accumulate five to ten times faster and contain five times as much organic carbon as red clay sediments. A more extensive discussion of the diagenesis of O_2, NO_3^-, solid organic carbon, and total nitrogen and ways to use these data to calculate the stoichiometry of the decomposing organic matter is presented in (9).

The shapes of the O_2 profiles at all of the stations indicate that there is a diffusive flux from the overlying water into the sediments. One can estimate this flux by using Fick's first law:

$$\text{Flux } O_2 = -D_{O_2,\,\text{pw}}\phi\left(\frac{dO_2}{dz}\right)_{z=0} \qquad (7)$$

where $D_{O_2,\,\text{pw}}$ is the average diffusion coefficient for O_2 in the pore water. The derivative of Eq. 1 was evaluated at $z = 0$ to obtain

$$\text{Flux } O_2 = D_{O_2,\,\text{pw}}\phi\, B\, \Delta O_2 \qquad (8)$$

We calculated the diffusive O_2 flux into the sediments, using Eq. 7 and the appropriate values of B and ΔO_2 for each station. The diffusion coefficient in situ [in square centimeters (bulk) per second] was approximated with the use of

$$D_{\text{pw}} = \frac{D_{\text{soln}}}{\phi \cdot F} \qquad (9)$$

where D_{soln} is the diffusion coefficient for O_2 in water [in square centimeters (water) per second], ϕ is the porosity [in cubic centimeters (water) per cubic centimeter (bulk)], and F is the formation resistivity factor [in centimeters (bulk) per centimeter (water)] (10). The value of D_{soln} at 5°C is 1.26×10^{-5} cm^2 sec^{-1} (11), and the average ϕ over the top 10 cm at these locations is about 0.90 (12). An estimate of the average tortuosity at $z = 0$ is $\theta = 2.0$ (13). Under these conditions, the $D_{O_2,\,\text{pw}}$ value used in the flux calculations is 6.0×10^{-6} cm^{-2} sec^{-1}. The diffusion flux estimates (Table 1) probably represent an upper limit as they have been calculated with the constraint that the O_2 content equals that of bottom water at $z = 0$. Careful inspection of the profiles in Fig. 2 reveals that many of the O_2 profiles could also be extrapolated to values less than that of bottom water at $z = 0$. Our diffusive O_2 fluxes are in good agreement with those calculated by Wilson (14) for the northeast Atlantic. His mean flux of 1.25×10^{-14} mole cm^{-2} sec^{-1} was also based on in situ samples.

Smith (15) and Hinga *et al.* (16) have measured the in situ O_2 uptake of deep-sea sediments in the North Atlantic and North Pacific. The O_2 consumption rates decrease by three orders of magnitude from the shallow sea floor to depths greater than 5000 m. Anomalously high values are found in sediments underlying surface waters with high productivity, such as the eastern and equatorial regions of the ocean basins. Unfortunately, we know of no direct O_2 uptake measurements from the region of our samples in the Pacific.

Smith attempted to divide his measurements in the North Atlantic into benthic community respiration (the part that is eliminated by Formalin treatment) and chemical O_2 demand (the part that remains). For depths deeper than 4000 m, he found no measurable chemical O_2 demand; his total O_2 uptake ranged from 0.02 to 0.09 ml m^{-2} hour^{-1}. By comparison, we measure an average O_2 flux of 0.08 ml m^{-2} hour^{-1} (Table 1), which is in good agreement with Smith's total O_2 demand. We argue, however, that if Formalin addition kills all the benthos, our measured O_2 gradients would still exist and our calculated O_2 fluxes into the sediments should be compared with the chemical O_2 demand. Smith's chemical O_2 demand should consist entirely of diffusion in aerobic sediments since reduced inorganic compounds should not be present in these sediments.

The mechanism of O_2 consumption in these sediments cannot be unequivocally resolved. It is clear that aerobic respiration with nitrification is the major microbial process occurring (9); however, there is no clear way to separate the respiration of larger organisms that reside in the sediments from respiration by bacteria.

If the average diffusion flux is about 9.0×10^{-14} mole cm^{-2} sec^{-1} and the area of aerobic pelagic sediments is 3.0×10^{18} cm^2 (17), then the total O_2 consumption rate due to diffusion below the sediment-water interface is about 8.3×10^{12} mole year^{-1}. This O_2 consumption must be considered in addition to O_2 consumption that occurs just at the sediment-water interface.

JAMES W. MURRAY
VARIS GRUNDMANIS*
Department of Oceanography,
University of Washington, Seattle 98195

References and Notes

1. M. L. Bender, K. A. Fanning, P. N. Froelich, G. R. Heath, V. Maynard, *Science* **198**, 605 (1977); S. Emerson, R. Jahnke, M. Bender, P. Froelich, G. Klinkhammer, C. Bowser, G. Setlock, *Earth Planet. Sci. Lett.*, in press.
2. G. Claypool and I. R. Kaplan, in *Natural Gases in Marine Sediments*, I. R. Kaplan, Ed. (Plenum, New York, 1974), p. 99; W. Stumm and J. J. Morgan, *Aquatic Chemistry* (Wiley-Interscience, New York, 1970), pp. 328–339.
3. F. L. Sayles, P. C. Mangelsdorf, Jr., T. R. S. Wilson, D. N. Hume, *Deep-Sea Res.* **23**, 259 (1976). The sampler that we used had 15 sampling ports over a 53-cm interval plus provision for the collection of a bottom water sample from about 0.5 m above the sediment-water interface. The sampling ports were located at 3-cm intervals down to a depth of 28 cm and 5-cm intervals thereafter. The total sample volume of 26 ml is

stored in 0.32-cm nylon pressure tubing. Because of capillary mixing, the usable volume is only about 16 ml.
4. All gas analyses were performed on a Hewlett-Packard dual-column gas chromatograph equipped with a sample stripping system and a Carle thermistor detector. The 4-ml sample is stripped with the carrier gas, which is then dried over Drierite; then O_2 + Ar are separated from the other gases on a 1.8-m molecular sieve 5A column at 40°C. The Ar and O_2 are not separated from each other, and thus a small correction for Ar must be made, based on the solubility of Ar in seawater.
5. At two stations, two gas-sampling valves were placed in series at every other depth to obtain an estimate of our overall precision. The mean difference between duplicate measurements was 7 μmole kg^{-1}. Accuracy was estimated by intercalibration against water column samples analyzed by Winkler titration. In addition, our bottom water measurements from the in situ sampler agree to within 2 percent with the Geochemical Ocean Sections Study (GEOSECS) bottom-water O_2 values for this part of the deep Pacific.
6. R. A. Berner, in *The Sea*, E. D. Goldberg, Ed. (Wiley, New York, 1974), vol. 5, pp. 427–450; *Early Diagenesis: A Theoretical Approach* (Princeton Univ. Press, Princeton, N.J., 1980).
7. T. L. Ku, W. S. Broecker, N. Opdyke, *Earth Planet. Sci. Lett.* **4**, 1 (1968).
8. N. L. Guinasso and D. R. Schink, *J. Geophys. Res.* **80**, 3022 (1975).
9. V. Grundmanis and J. W. Murray, *Geochim. Cosmochim. Acta*, in press.
10. R. E. McDuff and J. M. Gieskes, *Earth Planet. Sci. Lett.* **33**, 1 (1976).
11. A. Lerman, *Geochemical Processes: Water and Sediment Environments* (Wiley-Interscience, New York, 1979), p. 96.
12. Calculated from water content and sediment density measurements made by C. Olson and F. L. Sayles (Woods Hole Oceanographic Institution).
13. Estimated from resistivity measurements determined on sediment cores immediately after collection by C. Olson and F. L. Sayles.
14. T. R. S. Wilson, *Nature (London)* **274**, 354 (1978).
15. K. L. Smith, Jr., *Mar. Biol.* **47**, 337 (1978).
16. K. R. Hinga, J. M. Sieburth, G. R. Heath, *J. Mar. Res.* **37**, 557 (1979).
17. J. C. G. Walker, *Am. J. Sci.* **274**, 193 (1974).
18. We thank J. Sawlan for assistance in sample collection and M. Bolan for execution. Drs. S. Emerson, R. A. Berner, and F. L. Sayles offered many valuable, critical comments. We thank B. Fulton for typing the manuscript. University of Washington contribution number 1165. This research was supported by grant OCE-78 18746 from the National Science Foundation.

* Present address: Hawaii Loa College, Kaneohe, Oahu 96744.

19 March 1980; revised 15 May 1980

Surface Charge Heterogeneity in Amphibole Cleavage Fragments and Asbestos Fibers

Abstract. *Aspect ratio and electrophoretic mobility data for amphibole particles reveal that short fibers and blocky cleavage fragments have a smaller net charge than highly elongated particles. Asbestos fibers and cleavage fragments of the same dimensions exhibit the same net negative surface charge but positively charged ends and negatively charged lateral surfaces.*

Research is being done at the Bureau of Mines Twin Cities Research Center on the relation between electrophoretic mobility and the aspect ratio of amphibole fibers and cleavage fragments (*1*) in an effort to minimize the undesirable occupational hazards associated with mining and mineral processing operations. [The nomenclature used in this report conforms to that suggested by Campbell *et al.* (*2*).]

In order to determine the relation between surface charge and aspect ratio for a wide range of amphibole particle shapes, experiments were designed to determine both the surface charge and the aspect ratio for individual particles. In the work described here, a microelectrophoresis cell with a rectangular cross section was used so that particles in the field of view could be photographed. Electrophoretic mobility data were obtained for particles with aspect ratios from 1 up to 40. These data gave important insight into the surface charge properties of amphibole particles.

The asbestiform minerals studied were crocidolite and grunerite asbestos from the International Union Against Cancer (UICC) (*3*). A sample of acicular tremolite (originally from Canaan, Connecticut) was obtained from the Science Museum of Minnesota, St. Paul. The Bureau of Mines Research Center at Avondale, Maryland, supplied a sample of riebeckite from El Paso County, Colorado. The UICC samples were used as received, and the acicular tremolite and riebeckite were hand-ground in an agate mortar and pestle. Suspensions in distilled water [0.1 percent (weight-volume)] were prepared by magnetic stirring and ultrasonic agitation. The *p*H was adjusted to 7 with $0.01M$ HNO_3 and NaOH, and the mixtures were sealed and allowed to stand for 15 to 20 hours. If needed, the *p*H was readjusted to 7 just prior to the microelectrophoresis measurements.

Table 1. Limiting values of electrophoretic mobility resulting from the different lateral charge density and basal charge density.

Mineral	μ_2	μ_1
	(μm/sec)/(V/cm)	
Grunerite asbestos	−2.8	+5
Crocidolite	−2.8	+4
Fibrous tremolite	−2.5	+2
Riebeckite	−2.5	+1
All points	−2.7	+4

We determined the aspect ratio and surface charge simultaneously, using a rectangular cell electrophoresis system and petrographic microscope equipped with a camera. The rectangular cavity in the cell had a width of 12 mm and a depth of 0.95 mm. The polished platinum electrodes were separated by 7.4 cm, and the microscope had an overall magnification of ×375. The cell was filled with the suspension of amphibole particles and positioned so that the microscope was focused exactly 0.20 mm above the bottom of the cell.

Times were recorded only for elongated particles (aspect ratio of about 3 or greater) that remained parallel with the electric field as they moved. Blocky particles were randomly oriented owing to Brownian movement. The distance traveled was 220 μm, and the voltage was 175 V. The ionic strength was about 10^{-4} during these measurements. The shape, location, and orientation of each particle tracked was also recorded so that later it would be possible to determine which specific particle was followed in the resulting photograph. We determined the aspect ratio of each particle by measuring its image in the photograph; one photograph was required for each particle. Particles were usually 0.5 to 2 μm wide and 3 to 15 μm long.

A control experiment was performed to ensure that observed differences in mobility between elongated and blocky particles truly reflected a difference in net surface charge rather than simply a hydrodynamic effect. Grunerite asbestos and crocidolite were suspended in $10^{-3}M$ KNO_3. In both suspensions, the electrophoretic mobilities of blocky particles, elongated particles oriented perpendicular to the electric field, and elongated particles parallel with the field were measured.

For both grunerite asbestos and crocidolite, the elongated particles perpendicular to the electric field had relative electrophoretic mobilities of 0.74 ± 0.03 and 0.7 ± 0.02, respectively, compared with elongated particles parallel to the field. Theory predicts that the electrophoretic mobilities of spherical particles would exactly equal the mean of values of cylinders oriented parallel and perpendicular to the applied field (*4*). The blocky particles would approximate the behavior of spheres. Thus, on the basis of shape effects only, the mobility of blocky particles of grunerite asbestos and crocidolite were expected to be 0.85 ± 0.03 and 0.87 ± 0.04, respectively, relative to that of elongated particles moving parallel to the field. However, the observed

0036-8075/80/0926-1530$00.50/0